Check for updates

Energy Technology
Generation, Conversion, Storage, Distribution
www.entechnol.de

Characterization of Elasticity for Silicon-Containing Anodes by Microindentation

Hung Lin, Yuechen Wu, Burkhard Lewerich, Edwin Knobbe, Timo Danner, and Arnulf Latz*

The intricate internal stresses within porous electrode coatings (PEC) are induced by charging and discharging of lithium-ion batteries. The incorporation of silicon-based particles in the anode further exacerbates the volume change of active particles and the microstructure change of PECs during battery cycling. This highlights the urgent need for a mechanical model of the PEC in electrochemically and mechanically coupled cell simulations. The first step to develop such a model is a layer-resolved, homogenized mechanical characterization of the PEC. In cylindrical cells, the mechanical properties of the PEC are highly nonlinear due to its multiphase granular microstructure combined with its thin, rolled geometry inside the cell housing. Herein, microindentation is employed and analyzed to extract the one-dimensional mechanical response of a single PEC-layer. Three major challenges of microindentation, thermal drift, substrate effect, and tip size effect are overcome. Quantification of short-term elasticity as well as long-term viscoelasticity is done for a silicon-containing dry anode sample by the proposed workflow. The results demonstrate that microindentation is a suitable and effective measurement method for characterizing PECs, thereby facilitating the development of mechanical models for multidisciplinary cell simulations.

1. Introduction

The past decade has witnessed a remarkable surge in the electric vehicle market, driven by the increasing demand for cleaner and more efficient transportation solutions. At the forefront of this revolution lies the lithium-ion battery (LIB), which not only propelled the ongoing advancement but also raised challenges to academia and industry simultaneously.[1–3] LIBs are produced in different sizes and formats depending on the application. In recent years, cylindrical LIB cells have garnered substantial interest and attention within the automotive industry.[4] Cylindrical LIB cells consist of layers of electrodes and separators which are stacked, rolled, and placed into a metal housing. Electrodes are made of a current collector foil and a layer of porous electrode coating (PEC) on both sides, both with thickness in the length scale of 10^{-4}–10^{-6} m (The term "electrode" in this article refers to the complete cathode or anode structure, including the porous coating layer and current collector foil. The porous coating layer on the cathode or anode is specifically referred to as PEC). Electrolyte is filled into the cell after the electrodes and separators are placed in the cell, causing them to expand and completely fill the cavity between the jelly-roll and cell housing. During operation, internal stress of cells can go up to 10 MPa under normal condition.[5] It affects cell performance[6] and undergoes a periodical pattern of change during cycling since the PEC-layer expands and contracts during lithiation and delithiation.[7,8] To further enhance energy density, silicon-based particles have been incorporated in anodes.[9,10] The significantly larger volume change of the silicon-based active particles during battery operation poses major challenges such as pulverization and faster capacity fading,[11–13] highlighting the importance of thoroughly understanding the mechanical conditions in the battery cells during cycling.

Electrochemically and mechanically coupled (EMC) simulation is a powerful tool to understand and predict battery behavior that cannot easily be observed or measured. Zhang et al. combined

H. Lin
Faculty of Engineering
Computer Science and Psychology
Ulm University
Albert-Einstein-Allee 41, 89081 Ulm, Germany
E-mail: hung.lin@uni-ulm.de

The ORCID identification number(s) for the author(s) of this article can be found under https://doi.org/10.1002/ente.202500383.

© 2025 Bayerische Motoren Werke and The Author(s). Energy Technology published by Wiley-VCH GmbH. This is an open access article under the terms of the Creative Commons Attribution License, which permits use, distribution and reproduction in any medium, provided the original work is properly cited.

DOI: 10.1002/ente.202500383

H. Lin, Y. Wu, B. Lewerich, E. Knobbe
Battery Cell Competence Centre
Bayerische Motoren Werke Aktiengesellschaft
Petuelring 130, 80788 Munich, Germany

T. Danner, A. Latz
Institute of Engineering Thermodynamics
German Aerospace Center (DLR)
Pfaffenwaldring 38–40, 70569 Stuttgart, Germany

T. Danner, A. Latz
Helmholtz Institute Ulm for Electrochemical Energy Storage (HIU)
Helmholtzstraße 11, 89081 Ulm, Germany

A. Latz
Institute of Electrochemistry, Ulm University
Albert-Einstein-Allee 47, 89081 Ulm, Germany

a linear elastic mechanical model with an electrochemical-thermal model to study mechanical abuse-induced short circuit at the electrode level.[14] Sauerteig et al. established an EMC model to study ionic transport at macroscopic level. The used mechanical model is based on linear elasticity and includes also the particle expansion effect.[15] Pistorio et al. coupled an electrochemical and a linear elastic mechanical model to predict fractures in active materials.[16] To the authors' knowledge, most EMC simulations use linear elastic mechanical models. At particle level, this is a reasonable approach since the mechanical properties, e.g., NMC or silicon particles are close to linear elastic.[17–19] The mechanical behavior of the PEC-layer at electrode level is highly nonlinear due to its multiphase granular microstructure, which consists of active particles, binder, conductive additives, and pores.[18,20]

Another approach is to homogenize the PEC-layers in the jelly-roll, e.g., to focus on larger deformations of battery cells for automotive safety assessment. Ali et al. characterized a 10-stack electrode as a representative volume element (RVE) and modeled its mechanical behavior as elastic–plastic to study the microbuckling effect. In the elastic range, a linear elastic model is used where the apparent compression modulus is obtained from a constant-rate compression test.[21] Sahraei et al. used a crushable foam model to model a RVE of a complete set of cell components to study internal short circuit in battery cells.[22] Consequently, the main focus of these mechanical modeling efforts was on the yield criteria or failure mechanism, while the elastic properties were not fully resolved. Thus, the derived models were not suitable for EMC cell simulations, revealing a deficit for a suitable mechanical model to be used for such purposes.

The goal of this research is to establish a layer-resolved model for the mechanical properties of a PEC-layer in EMC cell simulations. The first step is to characterize the mechanical properties of a single PEC-layer, which is heavily influenced by the microstructure and appears to be viscoelastic due to the binder and conductive additives.[20,23] Universal testing machines (UTMs) are commonly used to characterize the microstructure of PEC-layers.[21,22,24] UTMs can easily perform uniaxial strain or uniaxial stress load cases. For instance, Brehm et al. characterized the cathode, separator, and anode layers of a LIB for the typical range of loads during battery operation.[25] However, the resolution of the sensors in UTMs is often insufficient to measure a single layer of electrode accurately. To overcome this limitation, electrodes need to be stacked for the measurement, which introduces potential errors. The measurement result is then post-processed under the assumption that the foil does not deform. Additionally, stacking electrodes requires more sample material, which is a significant drawback. To summarize, UTM measurements are straightforward but lack efficiency and accuracy, and introduce a source of potential errors due to electrode stacking.

In contrast, nanoindenters might be an ideal tool to mechanically characterize a single layer of electrode due to their high resolution. This mature method has already been used in researches characterizing mechanical properties of active particles, which requires even higher resolution than at electrode level. Vasconcelos et al. executed an instrumented grid nanoindentation on an NMC cathode and characterized the surface fraction, elastic modulus, and hardness of individual components in both dry and wet conditions.[18,26] Berla et al. also used nanoindentation on electrochemically lithiated silicon, whose Young's modulus was characterized to be 41 GPa and was found to creep readily.[17] To characterize the homogenized mechanical properties of a PEC-layer at electrode level, the standard sharp Berkovich tip is not suitable. Instead, flat indenter tips with diameter at the length scale of several hundred micrometers are used with a nanoindenter. Westphal et al.,[27] Sangrós Giménez et al.,[28] Scheffler et al.,[29] and Schreiner et al.[30–32] all used this method to characterize the mechanical responses of PEC-layers. Surprisingly, this method did not acquire a standardized terminology. To emphasize the length scale of the tip, which is the main distinction of this method from conventional nanoindentation with the sharp Berkovich tip, the term "microindentation" will be used in this article.

While microindentation has been employed in prior publications, it carries certain limitations that must be addressed before it can be effectively used to mechanically characterize a single PEC-layer. First, the size of the flat tip affects measurement results. It has to be proven that the microindentation can generate a one-dimensional load case, because the area of the flat tip is smaller than the sample surface. The more the tip radius approaches the sample thickness, the less the microindentation becomes a one-dimensional load case. The tip needs to be sufficiently large so that stress concentrations at the edge of the tip as well as sample deformations outside the flat tip can be neglected. In other words, the comparability of microindentation and the uni-axial strain load case needs to be proven. Second, thermal drift is a phenomenon experienced by nanoindenters due to their high resolution. The readout of tip displacement can drift w.r.t. time due to the small amount of heat generated from various sources, e.g., friction heat generated by the motion of stages or changes in environmental temperature. Thermal drift is not negligible during long-term measurements. As the displacement readout shifts, the viscoelastic characterization of the PEC-layer will be affected. Third, from preliminary experiments, we observed that the combined deformation of the layers underneath the PEC-layer, e.g., foil and glue, also contributes to non-negligible deformations during measurements. We will refer to this phenomenon as the substrate effect.

In this research, we examine the use of microindentation and apply it to characterize the elastic properties of a silicon-containing anode. In the next section, we address the tip size effect by comparing the measurement result of two different size tips and a series of finite element (FE) simulations. We further propose a measurement workflow that addresses the thermal drift and the substrate effect. Subsequently, we propose a load curve that can distinguish the measured short-term and long-term mechanical responses. In the "Result and Discussion" section, the proposed microindentation workflow is evaluated, and the characterized mechanical properties of the PEC-layer are presented.

2. Experimental Method

2.1. Equipment and Material

The "ZHN-Universal Nanomechanical Testing System" by ZwickRoell is used for this research, where a nanoindenter is installed on an active vibration damper in a special housing

 © 2025 Bayerische Motoren Werke and The Author(s). Energy Technology published by Wiley-VCH GmbH

21944296, 2025, 12, Downloaded from https://onlinelibrary.wiley.com/doi/10.1002/ente.202500383 by Dtsch Zentrum F. Luft-U. Raum Fahrt In D. Helmholtz Gemein., Wiley Online Library on [22/12/2025]. See the Terms and Conditions (https://onlinelibrary.wiley.com/terms-and-conditions) on Wiley Online Library for rules of use; OA articles are governed by the applicable Creative Commons License

with sound-dampening foam. The indenter tip is changeable. Microindentation experiments are performed on a single-side-coated anode that consists of silicon–carbon composite (40 wt%), graphite (54 wt%), carbon black (1.5 wt%), carbon nanotubes (0.01 wt%), and aqueous binder (4.49 wt%). After calendering, the thickness of the whole anode is 52 µm and the thickness of the PEC-layer is 41 µm, which are measured from a scanning electron microscopy (SEM) image in **Figure 1**a. A round sample with diameter $D = 18$ mm is punched from the anode sheet and fixed on a sample holder by an ethyl cyanoacrylate-based liquid glue on a glass surface to ensure complete flatness. The anode sample is dry and has never been in contact with electrolyte. The cylindrical flat tip used in the experiments is shown in Figure 1c. It is assumed that only the flat end is in contact with the sample during the complete indentation process, i.e., there is a constant contact area between tip and sample. Nominal stress σ_N is defined by the applied load over the contact area.

2.2. Measurement Protocol

2.2.1. Tip Size Effect

Two flat tips with different radii are selected to study the tip size effect: $R_{tip} = 150$ µm ("Tip S") and $R_{tip} = 250$ µm ("Tip L"). An identical load curve with σ_N-levels is applied on the sample with these 2 tips. The creep behavior that is measured with both tips will be compared. To further study the tip size effect, FE simulations of microindentation are performed with varying ratios between tip radius and sample thickness (R_{tip}/h). A linear elastic model with varying Poisson's ratios ν is used for the PEC-layer, because there is no commonly used mechanical model for PEC-layers. Using the linear elastic model for the PEC-layer leads to the worst-case scenario that microindentation deviates most from the one-dimensional load case, because the stress concentration at the tip edge becomes more pronounced. It is therefore suitable to use the linear elastic material model for the PEC-layer in these simulations to assess microindentations. The strain energy (SE) of a deformed sample is used to quantify the one-dimensionality of a microindentation. The effect of the tip size for various R_{tip} is shown by comparing the SE of a microindentation with the SE of a corresponding ideal uniaxial strain load case by Equation (1)

$$\Psi = \frac{SE_{micro-indentation}}{SE_{uniaxialstrain}} \tag{1}$$

For the case that the SE ratio Ψ approaches 1, we can neglect the tip size effect and model microindentation as one-dimensional uni-axial strain.

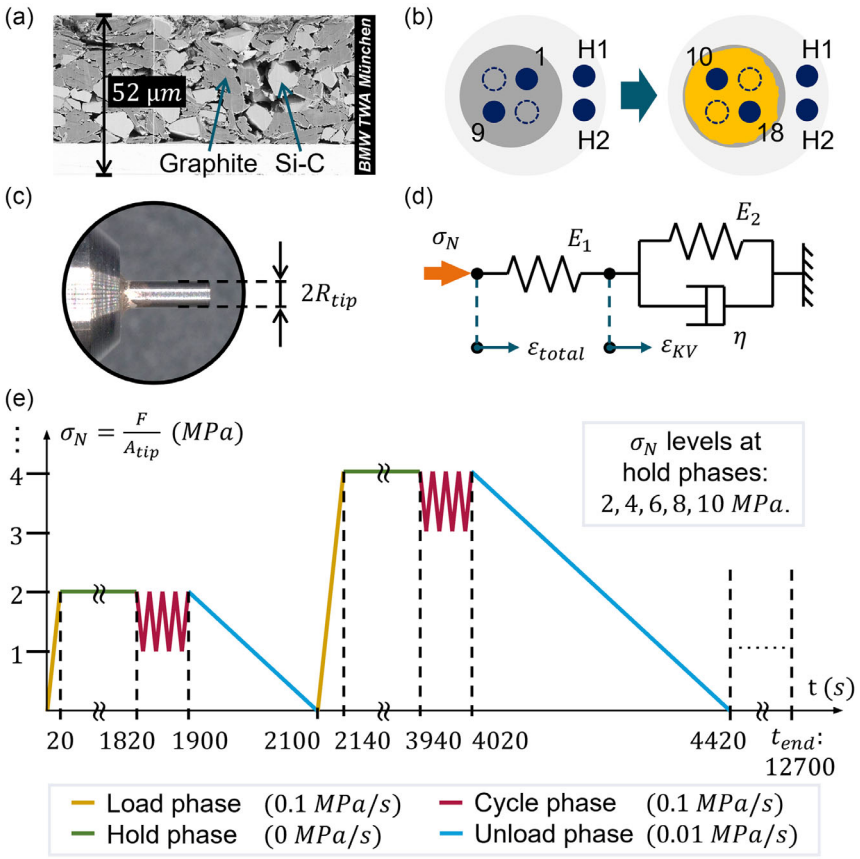

Figure 1. a) SEM image of the sample anode. b) Sequence of microindentation. First, 2 points on the glass sample holder surface are indented (H1, H2), followed by 9 points on the electrode (1 → 9), then the 2 points again on the glass basis. The anode coating layer is then removed, and microindentation is done with the same sequence but new points on the foil (H1, H2, 10 → 18, H1, H2). c) Picture of flat indenter tip. d) Standard linear solid model with Kelvin–Voigt representation. e) Load curve. Each σ_N-level consists of a load (yellow), hold (green), cycle (red), and unload (blue) phase.

 © 2025 Bayerische Motoren Werke and The Author(s). Energy Technology published by Wiley-VCH GmbH

21944296, 2025, 12, Downloaded from https://onlinelibrary.wiley.com/doi/10.1002/ente.202500383 by Dtsch Zentrum F. Luft-U. Raum Fahrt In D. Helmholtz Gemein., Wiley Online Library on [22/12/2025]. See the Terms and Conditions (https://onlinelibrary.wiley.com/terms-and-conditions) on Wiley Online Library for rules of use; OA articles are governed by the applicable Creative Commons License

21944296, 2025, 12, Downloaded from https://onlinelibrary.wiley.com/doi/10.1002/ente.202500383 by Dtsch Zentrum F. Luft-U. Raum Fahrt In D. Helmholtz Gemein., Wiley Online Library on [22/12/2025]. See the Terms and Conditions (https://onlinelibrary.wiley.com/terms-and-conditions) on Wiley Online Library for rules of use; OA articles are governed by the applicable Creative Commons License

2.2.2. Thermal Drift and Substrate Effect

The sequence of indentations shown in Figure 1b is used to correct for the thermal drift and substrate effect. Additional microindentations with an identical load curve are made on the hard surface of the sample holder before and after the actual indentation on the sample points to determine the thermal drift. The load curve contains holding phases (shown in green in Figure 1e). Assuming the glass surface and the flat tip do not creep during the holding phase, the displacement response of the sample holder during the holding phase can be used to obtain the thermal drift rate. The thermal drift rate during the actual indentation is interpolated between the rates measured before and after. The PEC-layer is removed after the indentation of the electrode is finished to assess the substrate effect. This reveals the foil of the current collector underneath, and the same load curve is applied on new points on the foil. The pure deformation of the PEC-layer is obtained by subtracting the substrate deformation from the electrode deformation. This post-process procedure is only applicable if the load case is one-dimensional, hence, the one-dimensionality of microindentations will be assessed in the result section.

2.2.3. Load Curve

It is not sufficient to characterize the elastic modulus by a simple load-unload profile, because the mechanical response of a PEC-layer is a combination of elastic, viscoelastic, and plastic material behavior. In this research, plasticity is excluded in our discussion because the focus is only on the material behavior during normal battery operation. Any deformation that does not recover immediately after unloading will be considered as a viscoelastic deformation. Figure 1e illustrates the microindentation load case. The total load profile consists of 5 sets to characterize a PEC-layer at different compression states. Each set has identical load rates and holding times, but they are performed at different σ_N-levels from 2 to 10 MPa. A hold phase is inserted between the load and the cycle phases in the load profile, to decouple the elastic, short-term, and the viscoelastic, long-term response of a PEC-layer. The load phase before a hold phase generates a combination of short and long-term responses, the hold phase shows only the long-term response, and the cycle phase can be modeled as short-term-only as the majority of long-term response is finished during the hold phase.

Before the load curve is applied on an indentation point, a surface finding process is performed by the nanoindenter. This process approaches the indenter tip to the sample surface at a constant velocity and defines the surface when the recorded force reaches 0.02 mN. Afterward, the load curve is applied at the defined sample surface.

2.3. Fitting of Results

A standard linear solid model based on a Kelvin–Voigt element (SLS-KV)[33,34] is shown in Figure 1d. This is used to fit the mechanical response of the PEC-layer and to analyze the viscoelastic behavior of our PEC sample. Equation (2) shows the stress–strain relation of a SLS-KV model where E_1, E_2, and η are constants.

$$\sigma_N = E_1(\varepsilon_{total} - \varepsilon_{KV}) = E_2\varepsilon_{KV} + \eta\dot{\varepsilon}_{KV} \quad (2)$$

It is important to note that our goal is not to fully reproduce the mechanical behavior of a PEC-layer using a complex model, but rather to demonstrate the trends of specific material behavior using a fundamental model. Hence, the SLS-KV model is not expected to capture the complete nonlinear viscoelastic behavior of the PEC-layer. It is sufficiently accurate for this work, because the main focus is to assess how viscoelasticity of PEC-layers can be measured and modeled by microindentations. The "GlobalSearch" function in MATLAB[35] is used to determine the parameters in the SLS-KV model. Objective is to minimize the root-mean-square error between the strain obtained from the SLS-KV model and the measured data.

3. Results and Discussion

3.1. Microindentation Method

3.1.1. Tip Size Effect

The apparent modulus E_{app} is a measure of the short-term mechanical response and is calculated with Equation (3)

$$E_{app} = (\sigma_{N,2} - \sigma_{N,1})/(\varepsilon_2 - \varepsilon_1) \quad (3)$$

For Equation (3), it is assumed that the chosen material behavior between state 1 and 2 is linear elastic. **Figure 2**b shows that the E_{app} obtained from results of Tip S is only 70 to 80% of that obtained from results of Tip L. In contrast, Figure 2a shows the creep displacement during the hold phase. In our load profile, the hold time for both Tip S and L are fixed at 1800 s, and the creep rate already slows down at the end of the hold phase when Tip L is used in the measurements but not in the case of Tip S. This trend is obvious at all σ_N-levels during the hold phase, meaning that a PEC-layer reaches a steady state faster with the larger Tip L when compared with the smaller Tip S. We are characterizing the short-term response of a PEC-layer based on the cycle phase of the load curve. It is directly after the hold phase, which is used to obtain the long-term response. Therefore, in the case of Tip S the creep of the PEC-layer is not fully developed, instead, the obtained E_{app} is a mixture of its short and long-term material response.

To analyze how the short-term response is affected by the tip size effect, we shall look into the FE simulation results. This reproduces only the short-term responses of the PEC-layer, because a linear elastic model is used. Figure 2c shows that Ψ approaches to 1 for large R_{tip}/h ratios independent of sample Poisson's ratio ν. To make the difference between microindentation and the uniaxial strain load case smaller than 10%, the ratio R_{tip}/h should be larger than 5. In conclusion, the tip size effect should be accounted for when using microindentation to characterize PEC-layers, as it can simultaneously affect the characterization of short and long-term responses.

Tip size effect of both short- and long-term responses can be explained by the region of influence during a microindentation. As Figure 2d illustrates, when the flat tip compresses the sample, not only the sample volume below (region I, yellow) but also a fraction of the sample outside the flat tip (region II, orange)

 © 2025 Bayerische Motoren Werke and The Author(s). Energy Technology published by Wiley-VCH GmbH

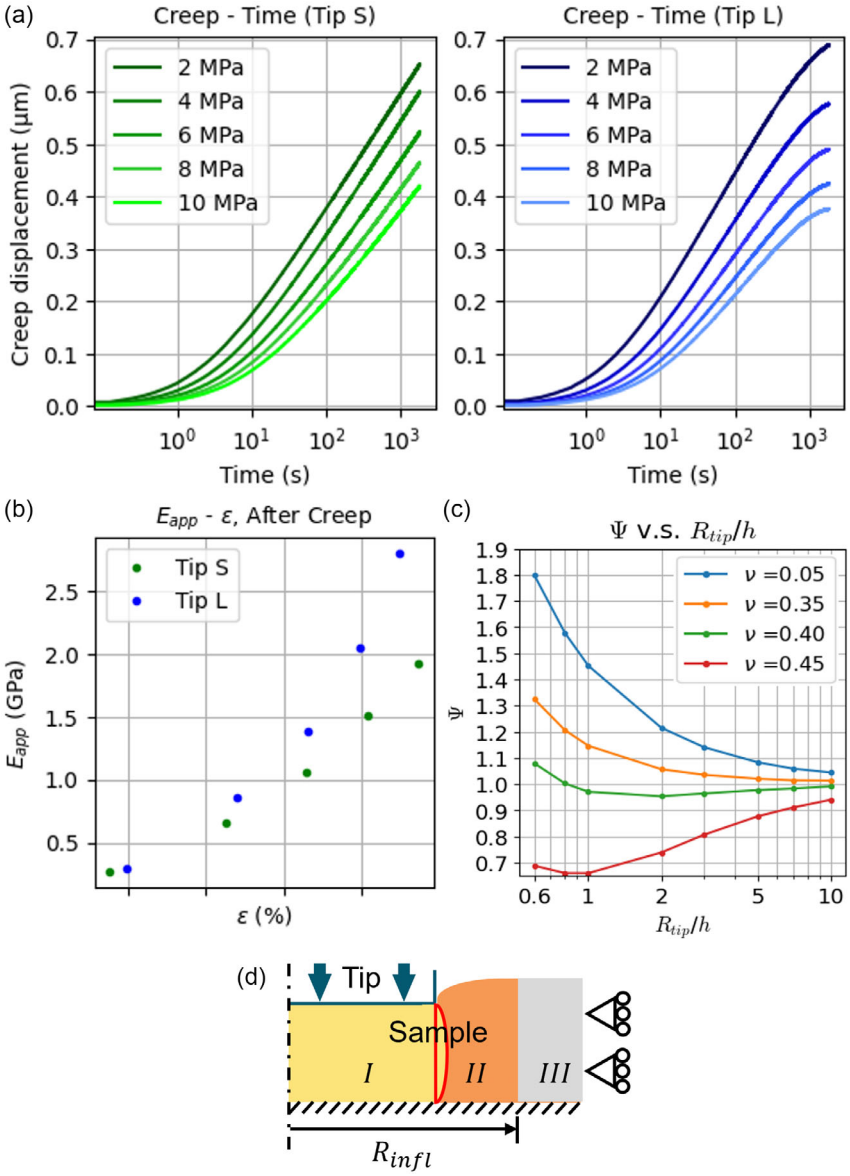

Figure 2. Result of the tip size effect. a) Creep displacement–time curve at various σ_N-levels for Tip S and Tip L. b) E_{app} obtained from the cycling phase measured by Tip S and Tip L. c) SE ratio $\Psi - R_{tip}/h$ results from FE simulation. d) Illustration of sample deformation under microindentation.

deforms. Region I and II combined is the region of influence during a microindentation. The material behavior in region II is also affecting the measurement, but it is difficult to include them in the modeling since the development of a mechanical model of the PEC-layer is work in progress. If we are modeling microindentation as a 1D-load case, the tip needs to be sufficiently large to reduce the error, i.e., the influence of region II must become negligible. In our experiments, it was possible to assess the characteristic creep time and to make the error for the short-term characterization smaller than 10% with the Tip L. Therefore, in the result section of mechanical behavior of the PEC-layer, we will extract and discuss the trend of short- and long-term mechanical properties of our anode coating sample based only on the measurement done with Tip L.

3.1.2. Thermal Drift and Substrate Effect

Figure 3a shows that the thermal drift rate changes rapidly at the beginning of an indentation series. Later, the thermal drift rates stabilize gradually as the nanoindenter reaches a new thermal equilibrium over time. Here, tests 1 and 2 are done by Tip S and Tip L, respectively. However, from our preliminary experiments, we see no clear evidence that the tip size affects the development of the thermal drift rate. Thus, we conclude that the difference of the thermal drift development in Figure 3a is caused by the slight difference of the environmental temperatures during the 2 tests. For our thermal drift compensation process, the absolute magnitude of the thermal drift is not a particularly meaningful metric. The critical consideration is

 © 2025 Bayerische Motoren Werke and The Author(s). Energy Technology published by Wiley-VCH GmbH

21944296, 2025, 12, Downloaded from https://onlinelibrary.wiley.com/doi/10.1002/ente.202500383 by Dtsch Zentrum F. Luft-U. Raum Fahrt In D. Helmholtz Gemein., Wiley Online Library on [22/12/2025]. See the Terms and Conditions (https://onlinelibrary.wiley.com/terms-and-conditions) on Wiley Online Library for rules of use; OA articles are governed by the applicable Creative Commons License

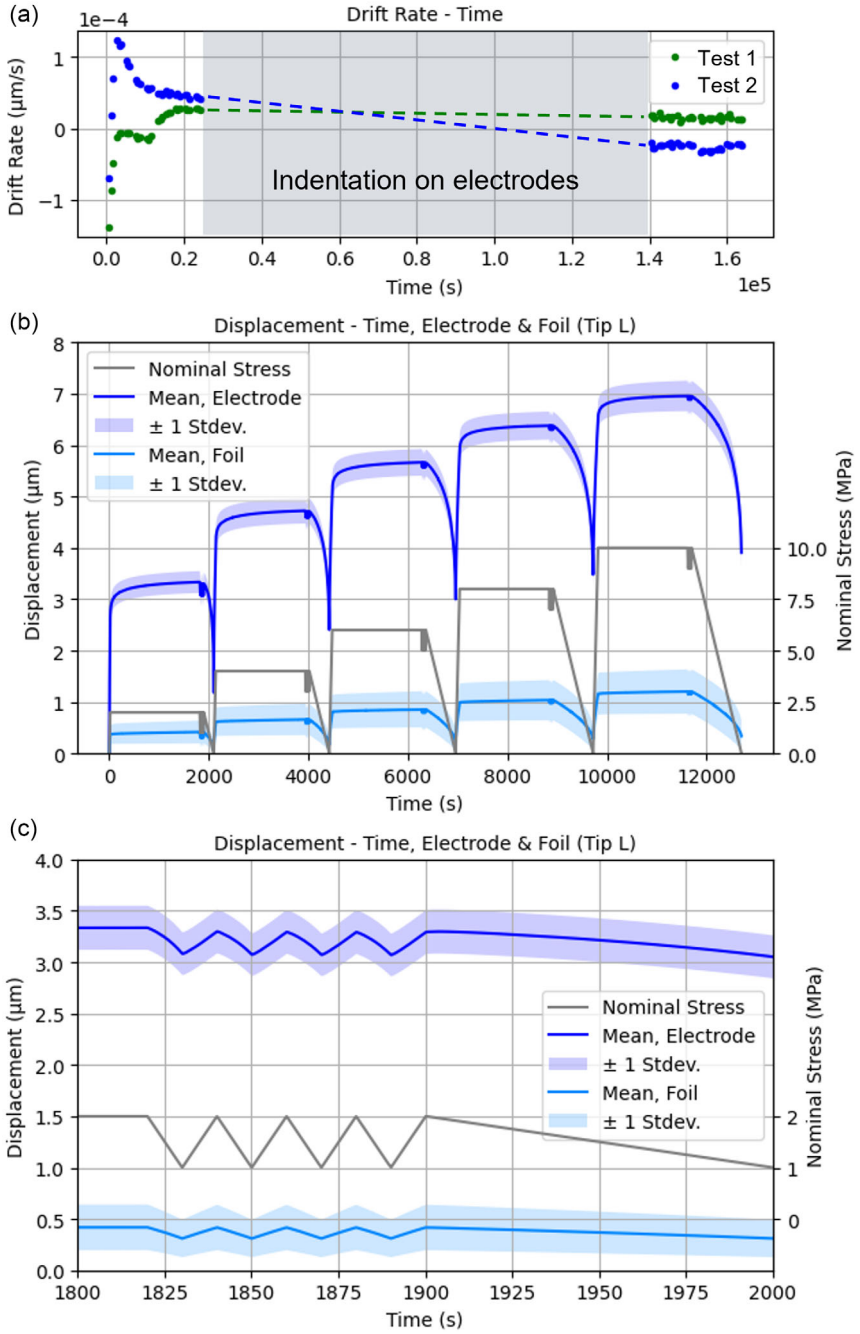

Figure 3. a) Thermal drift rate versus wall time of 2 microindentations on electrodes. The thermal drift rate during indentation (dashed line) is interpolated from the additional measurements before and after. b) Result of microindentation on electrode and foil. The mean and standard deviation of measured displacement-time data points of the electrode and foil by Tip L. c) Zoom-in of (b) during the cycle segment.

whether the evolution of the thermal drift rate remains stable over the course of the measurement. In case of Figure 3a, for both tests, the indenter already reached the phase of stable thermal drift development. When indenting electrodes, the actual thermal drift rate is not able to be measured by holding the load, because the electrode also sustains an amount of creep. We assume that the drift rate changes linearly during the indentation measurement based on the thermal drift before and after the indentation as the dashed lines in Figure 3a show, and the measured data are compensated accordingly. With the thermal drift rate shown in Figure 3a, the thermal drift-induced measurement error for test 1 over the measurement time of 10^4 s accumulates to 0.2 µm. For test 2, the measurement result would look tilted because the drift rate is evolving during the measurement period.

Figure 3b shows the mean value and standard deviation of 9 indentations done on one electrode and 8 indentations done on

 © 2025 Bayerische Motoren Werke and The Author(s). Energy Technology published by Wiley-VCH GmbH

21944296, 2025, 12, Downloaded from https://onlinelibrary.wiley.com/doi/10.1002/ente.202500383 by Dtsch Zentrum F. Luft-U. Raum Fahrt In D. Helmholtz Gemein., Wiley Online Library on [22/12/2025]. See the Terms and Conditions (https://onlinelibrary.wiley.com/terms-and-conditions) on Wiley Online Library for rules of use; OA articles are governed by the applicable Creative Commons License

one foil with Tip L. In case of the foil, 1 outlier is excluded due to significant mismatching result after thermal drift correction. The zero point of displacement is defined at $\sigma_N = 0.1$ MPa during the first loading phase to prevent errors in a surface detection procedure required due to the rough surface of a PEC-layer. Comparison of the compression depth between electrode indentation and foil indentation in Figure 3b shows that at every stage, 10–20% of the measured indentation is in the foil and glue layer beneath. Hence, it is clear that the deformation of the substrate below a PEC-layer is not negligible, and a procedure to account for the indentation of the foil is required. The coefficient of variation (CV) of the electrode indentation is around 10% at the start and gradually decreases to less than 5% as the indentation goes deeper. In the cycle segment shown in Figure 3c, the lower and upper bound of the ± 1 standard deviation looks similar to directly shifting the mean curve up and down, because the slopes of the sawtooth part of all 9 measurements are almost identical. In case of the measurements on the foil, the CV is larger during the complete measurement at around 50%. However, the CV is almost not changing during the different segments in the measurement. The displacement of foil indentations is far smaller than electrode indentations. This indicates that the surface finding process of the nanoindenter could be the main error source when using a flat tip to indent a foil. The measured mechanical response displays a high level of reproducibility when the applied load or compression depth increases. Post-processing of results from the electrode and foil is required to obtain the response of the PEC-layer only. The CV of the post-processed PEC-layer deformation is around 10%, which indicates high precision and good applicability of microindentation to mechanically characterize PECs.

3.2. Mechanical Behavior of the PEC-Layer

Figure 4a shows both the short- and long-term indentation measurements of the PEC at different compression depths after correction for the thermal drift and substrate effect. For instance, at the first σ_N-level shown in Figure 4b, we can observe 2 different apparent elastic moduli E_{app} before and after creep. In the cycle phase, the stress–strain curve almost perfectly align on top of each other for different load cycles, which indicates that the captured mechanical response is almost only short term. The effect of the long-term response is still present and is displayed by the hysteresis of the curve. However, during the cycle phase, the highest and lowest strains are nearly unchanged at 7 and 6.75%. Before the holding phase, a mixture of short- and long-term mechanical response is observed and cannot be decoupled, thus, it is critical to design the loading profile accordingly to characterize the needed mechanical property.

3.2.1. Long-Term Mechanical Properties

We employ the SLS-KV model depicted in Figure 1d to analyze the long-term mechanical response of the PEC-layer shown in Figure 4a. The load phases cannot be effectively captured by the SLS-KV model with constant spring coefficients since the PEC-layer exhibits a stiffening effect while being compressed. We will revisit this data in the discussion of short-term responses but exclude the load phase from the discussion of the long-term mechanical properties. Instead, we focus on separately fitting the hold and the cycle phases at each σ_N-levels.

In **Figure 5**a,c, a SLS-KV model is fitted to the holding sections of $\sigma_N = 2$ and 10 MPa, respectively. Interestingly, the optimal parameter set obtained with the global search algorithm exhibits a consistent characteristic. The strain at the start of the holding phase is completely accounted for by the primary spring (E_1 in Figure 1d), and the KV-element is only responsible for the strain generated during the holding phase. At first glance, the creep behavior seems to be accurately reproduced. However, in Figure 5a, it can be observed that even after the strain of SLS-KV stabilizes, the measured PEC strain continues to increase slowly. Therefore, the PEC-layer creeps, but the creeping behavior is too complicated to be modeled by a single KV-element. Figure 5b shows the cycle segment for $1 \leq \sigma_N \leq 2$ MPa, and Figure 5d shows the cycle segment for $9 \leq \sigma_N \leq 10$ MPa. The model successfully replicates the amplitude of the oscillation as well as the simultaneous slow reduction in the strain. The amplitude of oscillation is the short-term response and is captured by the primary spring with E_1. The decay of the strain curve is the long-term response and is captured by the KV-element. It is also evident that the curvature of each individual sawtooth is not

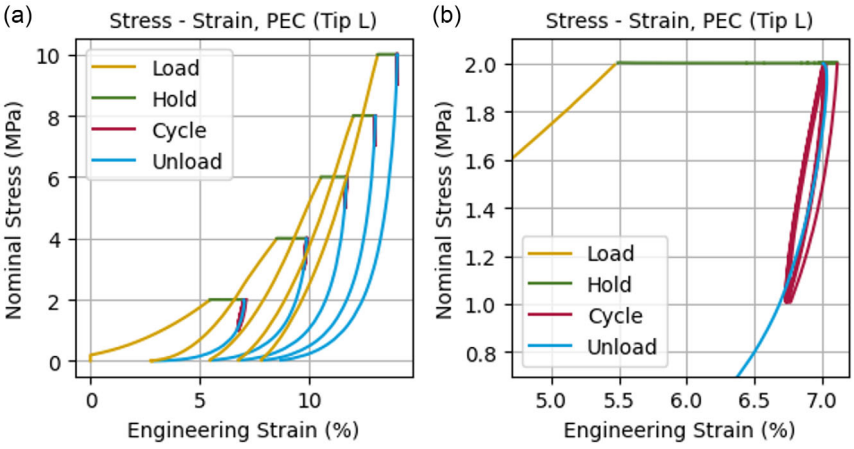

Figure 4. a) Stress–strain curve of pure anode coating under microindentation with Tip L under different σ_N-levels. b) Zoom of (a) at the first σ_N-level.

 © 2025 Bayerische Motoren Werke and The Author(s). Energy Technology published by Wiley-VCH GmbH

21944296, 2025, 12, Downloaded from https://onlinelibrary.wiley.com/doi/10.1002/ente.202500383 by Dtsch Zentrum F. Luft-U. Raum Fahrt In D. Helmholtz Gemein., Wiley Online Library on [22/12/2025]. See the Terms and Conditions (https://onlinelibrary.wiley.com/terms-and-conditions) on Wiley Online Library for rules of use; OA articles are governed by the applicable Creative Commons License

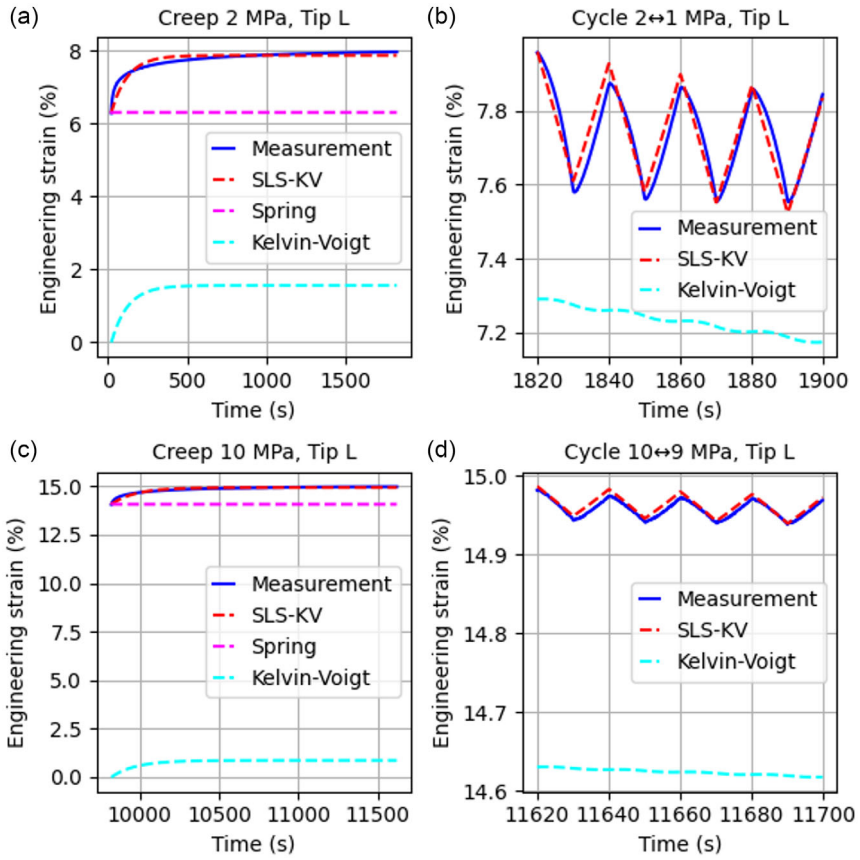

Figure 5. SLS-KV model fitted in a) $\sigma_N = 2$ MPa hold phase, b) cycle phase with $1 \leq \sigma_N \leq 2$ MPa, c) $\sigma_N = 10$ MPa hold phase, and d) cycle phase with $9 \leq \sigma_N \leq 10$ MPa of Tip L.

accurately replicated by the model. This could be attributed to the presence of multiple stages of viscoelastic behavior in the PEC-layer, which cannot be fully captured by a single KV-element. Figure 5 demonstrates that the PEC-layer exhibits clear viscoelastic characteristics. However, the nonlinear viscoelasticity, with an increasing elastic modulus during compression, cannot be adequately modeled using a simple SLS-KV model.

The retardation time τ, defined by Equation (4), is the characteristic time for the KV-element

$$\tau = \eta / E_2 \tag{4}$$

where η is the damper coefficient and E_2 is the spring coefficient of the parallel spring in Figure 1d.

Figure 6 shows the fitted $\tau - \varepsilon$ parameters based on the SLS-KV model for each σ_N-level. ε on the x-axis is defined as the initial strain of each fitting section. Figure 6a is the result of the holding phase. In the graph, τ increases almost linearly as function of strain. The τ values at different strains are critical for developing a mechanical model for a PEC-layer since this is a direct quantification of viscoelasticity. Figure 6b shows the result of the cycle segment. Here, τ increases linearly for the first 3 points and changes only marginally for the last 2 points. A possible explanation could be the deformation of the porous granular microstructure. When indented deep enough, there will be no more possible pore closure, the microstructure is thus fixed, and further deformation is achieved by particle deformation solely. Since the microstructure is fixed, its intrinsic mechanical properties including τ stay similar. Comparing Figure 6a,b, it is obvious that the τ values in the holding phase are one order smaller than those in the cycle segment. This could indicate significant microstructure change during creep or the existence of plasticity.

3.2.2. Short-Term Mechanical Properties

We conclude the discussion with the short-term response of a PEC-layer to a mechanical load. **Figure 7** shows $E_{app} - \varepsilon$ of a PEC-layer at different engineering strains computed from Figure 4a, assuming the stress–strain curve is linear in every computing interval. E_{app} is discussed here because we are analyzing the results under the assumption of a uniaxial strain load case, in which the Poisson's ratio of the sample also affects its stiffness when being compressed. However, we currently do not have any lateral force or displacement measurements as reference. Thus, the complete material behavior, namely the "apparent" elastic modulus, is discussed. Figure 7a shows $E_{app} - \varepsilon$ before the holding phase. The interval from the measurement that is used to compute E_{app} is obtained from the section of $\sigma_{N,creep} - 1\,\text{MPa} \rightarrow \sigma_{N,creep}$ in the load segment. During the load

 © 2025 Bayerische Motoren Werke and The Author(s). Energy Technology published by Wiley-VCH GmbH

21944296, 2025, 12, Downloaded from https://onlinelibrary.wiley.com/doi/10.1002/ente.202500383 by Dtsch Zentrum F. Luft-U. Raum Fahrt In D. Helmholtz Gemein., Wiley Online Library on [22/12/2025]. See the Terms and Conditions (https://onlinelibrary.wiley.com/terms-and-conditions) on Wiley Online Library for rules of use; OA articles are governed by the applicable Creative Commons License

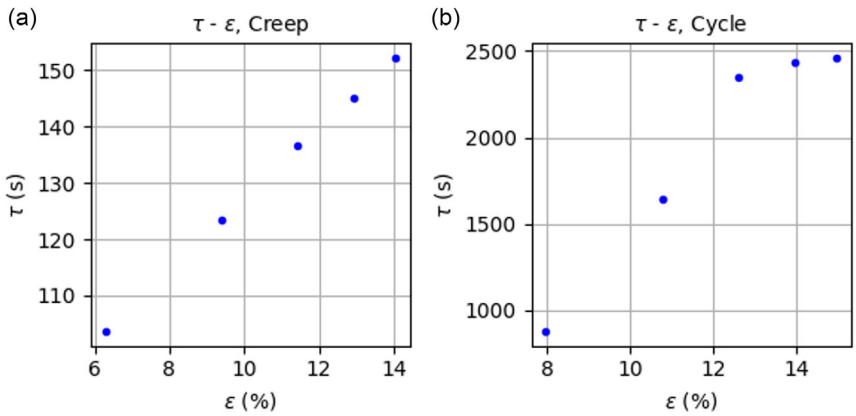

Figure 6. a) Fitted τ value at various σ_N-levels versus strain in the holding phases. b) Fitted τ value at various σ_N-levels versus strain in the cycle segment.

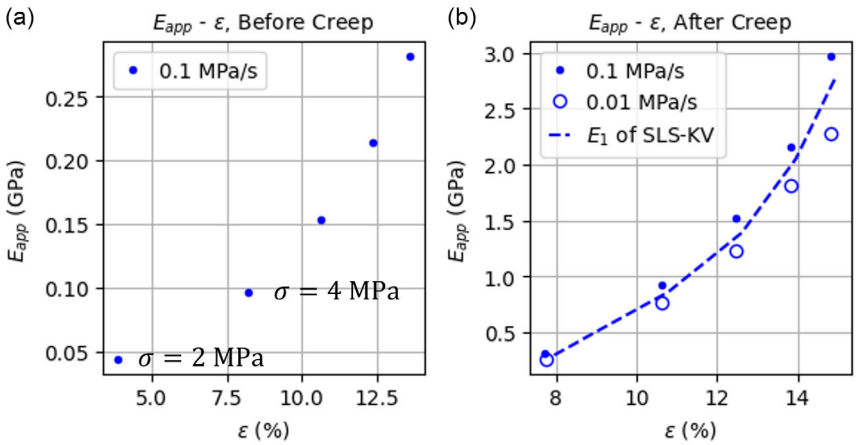

Figure 7. $E_{app} - \varepsilon$ a) before the holding phase, b) after the holding phase. Data points 0.1 MPa s^{-1} are taken from the cycle segment and 0.01 MPa s^{-1} from the unload segment. E_1 of SLS-KV are the parameters fitted from the cycle segment.

segment, the load rate is fixed at 0.1 MPa s^{-1}. Figure 7b shows $E_{app} - \varepsilon$ after the holding phase. In this graph, the curve of rate 0.1 MPa s^{-1} is obtained from the cycle segment, the curve of rate 0.01 MPa s^{-1} is obtained from the section of $\sigma_{N,creep} \rightarrow \sigma_{N,creep} - 1$ MPa of the unload segment. Comparing Figure 7a,b, all E_{app} values in Figure 7b are significantly larger. Before the holding phase, a mixture of short and long-term responses of the PEC-layer is captured, showing a much softer material behavior. After the long-term response is finished in the holding phase, we could capture only the short-term mechanical response, which results in a higher E_{app} after the holding phase. However, Figure 7b shows that E_{app} also depends on the loading or unloading rate after creep. With a slower rate, the obtained E_{app} is smaller. E_1 is the coefficient of the primary spring in the SLS-KV model fitted in the cyclic load interval, e.g., see Figure 5b,d. The similarity of E_1 and the two other measured E_{app} shows that the mechanical response of a PEC-layer can be modeled as short-term-only after creep is done.

In Brehm et al.,[25] anode stacks with pure graphite undergo a UTM compression test at a rate of 0.017 MPa s^{-1}. The obtained E_{app} is around 400 and 600 MPa at a compression stress of 1.0 and 3.0 MPa, respectively. This load case is comparable to the unload phase shown in Figure 1e, and we obtained an E_{app} of 270 and 760 MPa under a nominal stress of 2.0 and 4.0 MPa, as shown in Figure 7b. Although the composition of the used anode sample is different, it is reasonable that the obtained E_{app} has the same order of magnitude. Thus, the mechanical property of the active particles is not the sole factor of the overall mechanical response of the PEC-layer, but also the porous microstructure and the binder phase.

Due to the binder phase and the porous granular microstructure of PECs, viscoelasticity cannot be neglected during mechanical characterization. The load case of the mechanical characterization process must be designed in a certain way to take viscoelasticity into consideration. Although at the same engineering strain, E_{app} after the holding phase is multiple times larger than before the holding phase. This indicates that the mechanical behavior of a PEC-layer might be path dependent. For instance, at engineering strain of 12.5%, E_{app} is around 210 MPa before the holding phase but 1.0–1.5 GPa after the holding phase. In conclusion, the mechanical behavior of a PEC-layer is indeed highly nonlinear and shows different responses

 © 2025 Bayerische Motoren Werke and The Author(s). Energy Technology published by Wiley-VCH GmbH

21944296, 2025, 12, Downloaded from https://onlinelibrary.wiley.com/doi/10.1002/ente.202500383 by Dtsch Zentrum F. Luft-U. Raum Fahrt In D. Helmholtz Gemein., Wiley Online Library on [22/12/2025]. See the Terms and Conditions (https://onlinelibrary.wiley.com/terms-and-conditions) on Wiley Online Library for rules of use; OA articles are governed by the applicable Creative Commons License

depending on how the measurement is designed. When conducting measurements to obtain material parameters for mechanical simulations, it is crucial to ensure that the measurement conditions, setups, and load rates accurately reflect the real-world scenario of interest.

3.3. Limitation of Microindentation

There are still limitations and unique characteristics of the microindentation method that one needs to bear in mind. First, the microindentation method only measures a relatively small area compared to the UTM, i.e., the characterization is local. This could be beneficial for scenarios like studying the local effects or unevenness of the calendering process. However, for characterizing the homogenized mechanical behavior, it could be argued that we need to take multiple measurements at different areas of the sample, so the local fluctuations can be eliminated statistically, as done in this article. The second limitation of microindentation is the definition of the sample surface. Before the indentation starts, the indenter tip approaches the surface until the surface definition force threshold is reached. Once reached, the nanoindenter defines this point of depth as the surface of the sample. After calendering, the surface of the electrode sheet is not completely flat because the microstructure of the PEC-layer springs back, resulting in local "pop ups" of active particles. When indenting the PEC-layer with a flat tip, the surface definition force threshold can be reached early when a small portion of the "pop ups" contacts the flat tip. This results in an unusually soft contact behavior in the beginning of the indentation. In this article, the default setting from the nanoindenter of the surface definition force threshold is used, which is 20 μN. For Tip L, it corresponds to 10^{-4} MPa. However, this default setting is designed for characterizing thin, hard films with a sharp tip, which is different from characterizing PEC-layers with a flat tip. We therefore recommend a higher value of the surface definition force threshold to characterize the homogenized behavior of the PEC-layer and a lower value to characterize the local effects.

4. Conclusion

In our article, we could show that microindentation is a robust, realistic, efficient, and suitable mechanical characterization method for PEC-layers. Mechanical measurements are performed using a nanoindenter with a micrometer-sized tip. To perform accurate measurements, three challenges have been overcome in the research. First, thermal drift is compensated with the help of additional indentations on the sample holder before and after the actual indentation of the sample. Second, mechanical response of only the PEC-layer is extracted by doing additional indentations on the foil after indenting the electrode. Third, tip size effects affect both short and long-term measurement and can be reduced by choosing the right tip diameter depending on the sample height. We conclude that modeling the measurement result by Tip L as one-dimensional uniaxial strain load case is an adequate representation of the PEC. The measurement result of a PEC-layer done by the proposed microindentation procedure shows that PEC's mechanical response always consists of elastic and viscoelastic behavior. Based on an analyze with a SLS-KV model, we conclude that short-term mechanical properties of a PEC-layer can be characterized once the long-term response is determined. The increase of PEC's short-term E_{app} during compression is characterized.

Finally, multidisciplinary cell simulations are powerful tools to support the LIB development process. With correct usage and awareness of its limit, the microindentation method can provide necessary layer-resolved material characterizations for the development of the required mechanical model. We anticipate that the microindentation method will be incorporated into characterization methods as part of battery research, such as the characterization of wetted, charged, cycled, and aged LIB electrodes or even solid-state battery electrodes.

Acknowledgements

The authors would like to express their gratitude to Dr. Thomas Chudoba from Advanced Surface Mechanics GmbH and Mr. Michael Heier from ZwickRoell GmbH for their valuable technical assistance regarding the setup of the nanoindenter. The authors also appreciate the kindness of their BMW colleagues Dr. Lu Jin for providing the anode sample and Shu-Wei Chen for taking the SEM picture of their sample. Finally, the authors extend their sincere thanks to colleagues at HIU and BMW for their insightful discussions.

Open Access funding enabled and organized by Projekt DEAL.

Conflict of Interest

The authors declare no conflict of interest.

Data Availability Statement

The data that support the findings of this study are available from the corresponding author upon reasonable request.

Keywords

indentation, lithium-ion batteries, mechanical properties, silicon, viscoelasticity

Received: February 27, 2025
Revised: June 24, 2025
Published online: September 8, 2025

[1] G. E. Blomgren, *J. Electrochem. Soc.* **2016**, *164*, A5019.
[2] C. Xu, Q. Dai, L. Gaines, M. Hu, A. Tukker, B. Steubing, *Commun. Mater.* **2020**, *1*, 99.
[3] J. Deng, C. Bae, A. Denlinger, T. Miller, *Joule* **2020**, *4*, 511.
[4] S. Baazouzi, N. Feistel, J. Wanner, I. Landwehr, A. Fill, K. P. Birke, *Batteries* **2023**, *9*, 309.
[5] R. Li, W. Li, A. Singh, D. Ren, Z. Hou, M. Ouyang, *Energy Storage Mater.* **2022**, *52*, 395.
[6] W. Li, Y. Xia, J. Zhu, H. Luo, *J. Electrochem. Soc.* **2018**, *165*, A1537.
[7] X. Wang, Y. Sone, S. Kuwajima, *J. Electrochem. Soc.* **2004**, *151*, A273.
[8] J. Cannarella, C. B. Arnold, *J. Power Sources* **2014**, *245*, 745.
[9] Y. Hu, R. Demir-Cakan, M. Titirici, J. Müller, R. Schlögl, M. Antonietti, J. Maier, *Angew. Chem., Int. Ed.* **2008**, *47*, 1645.
[10] R. Schmuch, R. Wagner, G. Hörpel, T. Placke, M. Winter, *Nat. Energy* **2018**, *3*, 267.

 © 2025 Bayerische Motoren Werke and The Author(s). Energy Technology published by Wiley-VCH GmbH

21944296, 2025, 12, Downloaded from https://onlinelibrary.wiley.com/doi/10.1002/ente.202500383 by Dtsch Zentrum F. Luft-U. Raum Fahrt In D. Helmholtz Gemein., Wiley Online Library on [22/12/2025]. See the Terms and Conditions (https://onlinelibrary.wiley.com/terms-and-conditions) on Wiley Online Library for rules of use; OA articles are governed by the applicable Creative Commons License

[11] C. K. Chan, H. Peng, G. Liu, K. McIlwrath, X. F. Zhang, R. A. Huggins, Y. Cui, *Nat. Nanotechnol.* **2007**, *3*, 31.
[12] H. Jia, X. Li, J. Song, X. Zhang, L. Luo, Y. He, B. Li, Y. Cai, S. Hu, X. Xiao, C. Wang, K. M. Rosso, R. Yi, R. Patel, J.-G. Zhang, *Nat. Commun.* **2020**, *11*, 1474.
[13] Y. Wang, M. Satoh, M. Arao, M. Matsumoto, H. Imai, H. Nishihara, *Sci. Rep.* **2020**, *10*, 3208.
[14] C. Zhang, S. Santhanagopalan, M. A. Sprague, A. Pesaran, *ECS Trans.* **2016**, *72*, 9.
[15] D. Sauerteig, N. Hanselmann, A. Arzberger, H. Reinshagen, S. Ivanov, A. Bund, *J. Power Sources* **2018**, *378*, 235.
[16] F. Pistorio, D. Clerici, F. Mocera, A. Somà, *J. Power Sources* **2023**, *580*, 233378.
[17] L. A. Berla, S. W. Lee, Y. Cui, W. D. Nix, *J. Power Sources* **2015**, *273*, 41.
[18] L. S. de Vasconcelos, R. Xu, J. Li, K. Zhao, *Extreme Mech. Lett.* **2016**, *9*, 495.
[19] Y. Wang, Q. Zhang, D. Li, J. Hu, J. Xu, D. Dang, X. Xiao, Y. Cheng, *Adv. Energy Mater.* **2018**, *8*, 1702578.
[20] P. Gupta, B. Üçel, P. Gudmundson, E. Olsson, *Exp. Mech.* **2020**, *60*, 847.
[21] M. Y. Ali, W.-J. Lai, J. Pan, *J. Power Sources* **2013**, *242*, 325.
[22] E. Sahraei, E. Bosco, B. Dixon, B. Lai, *J. Power Sources* **2016**, *319*, 56.
[23] Z. Chen, L. Christensen, J. R. Dahn, *J. Appl. Polym. Sci.* **2003**, *90*, 1891.
[24] C. Zhang, J. Xu, L. Cao, Z. Wu, S. Santhanagopalan, *J. Power Sources* **2017**, *357*, 126.
[25] J. Brehm, A. Durdel, T. Kussinger, P. Kotter, M. Altmann, A. Jossen, *Batteries* **2024**, *10*, 422.
[26] L. S. de Vasconcelos, N. Sharma, R. Xu, K. Zhao, *Exp. Mech.* **2018**, *59*, 337.
[27] B. Westphal, H. Bockholt, T. Günther, W. Haselrieder, A. Kwade, *ECS Trans.* **2015**, *64*, 57.
[28] C. Sangrós Giménez, B. Finke, C. Nowak, C. Schilde, A. Kwade, *Adv. Powder Technol.* **2018**, *29*, 2312.
[29] S. Scheffler, R. Jagau, N. Müller, A. Diener, A. Kwade, *Batteries* **2022**, *8*, 46.
[30] D. Schreiner, A. Klinger, G. Reinhart, *Proc. CIRP* **2020**, *93*, 149.
[31] D. Schreiner, J. Lindenblatt, F. J. Günter, G. Reinhart, *Proc. CIRP* **2021**, *104*, 91.
[32] D. Schreiner, J. Lindenblatt, R. Daub, G. Reinhart, *Energy Technol.* **2022**, *11*, 2200442.
[33] R. Xiao, H. Sun, W. Chen, *Mech. Mater.* **2016**, *100*, 148.
[34] Q. Hao, S. Greenhalgh, *Geophys. J. Int.* **2019**, *219*, 1939.
[35] T. M. Inc., MATLAB Version: 23.2.0.2485118 (R2023b) Update 6 **2023**.

 © 2025 Bayerische Motoren Werke and The Author(s). Energy Technology published by Wiley-VCH GmbH

21944296, 2025, 12, Downloaded from https://onlinelibrary.wiley.com/doi/10.1002/ente.202500383 by Dtsch Zentrum F. Luft-U. Raum Fahrt In D. Helmholtz Gemein., Wiley Online Library on [22/12/2025]. See the Terms and Conditions (https://onlinelibrary.wiley.com/terms-and-conditions) on Wiley Online Library for rules of use; OA articles are governed by the applicable Creative Commons License